Thermal Science and Engineering Progress 55 (2024) 102884

Contents lists available at ScienceDirect

Thermal Science and Engineering Progress

journal homepage: www.sciencedirect.com/journal/thermal-science-and-engineering-progress

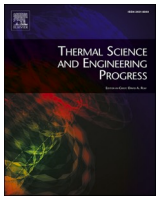

Thermoelectric generator efficiency: An experimental and computational approach to analysing thermoelectric generator performance

Qusay Doraghi [a], Hussam Jouhara [a,b,*]

[a] Heat Pipe and Thermal Management Research Group, College of Engineering, Design and Physical Sciences, Brunel University London, UB8 3PH, UK
[b] Vytautas Magnus University, Studentu Str. 11, LT-53362 Akademija, Kaunas Distr., Lithuania

ARTICLE INFO

Keywords:
Waste heat recovery
Thermoelectric generators (TEGs)
Experimental validation
COMSOL multiphysics
Computational simulation
Heat transfer

ABSTRACT

TEGs are devices that convert heat directly into electricity through the Seebeck effect, offering a promising solution for waste heat recovery in various industries. In this research, COMSOL Multiphysics 6.0 was used to conduct a comprehensive 3-dimensional computational study of TEGs. Integrating thermal and electrical models in COMSOL facilitates a detailed understanding of the thermoelectric phenomenon. Applying six distinct temperature gradients, temperature and electrical distribution, power output, and efficiency of the TEG was thoroughly analysed. Experimental validation confirms strong agreement between simulation and experimental data, emphasizing accuracy. The average efficiency for the TEG at 1 Ω load is 3.12 %, increasing to 3.62 % for a 2 Ω load. The relative error between the computational model and the experimental model was 5 % for open circuit, 12.56 % for closed circuit at 1 Ω, and 12.14 % for closed circuit at 2 Ω, affirming the accuracy of the computational approach. Therefore, the computational model is validated by experimental results.

Moreover, the findings highlight the relationship between external load resistance and power output, revealing that the maximum output power was achieved when the external load resistance matched the internal load resistance at 2 Ω. This work also significantly contributes to advancing the computational modelling of TEGs, validated through rigorous experimental analysis.

1. Introduction

The increasing demand for energy worldwide makes it essential to develop novel technologies that improve energy efficiency and reduce dependency on fossil fuels [1–3]. The Announced Pledges Scenario (APS) forecasts a 7,000 TWh global energy consumption increase, while the Stated Policies Scenario (STEPS) projects a rise of 5,900 TWh. Growing markets demand more power due to factors such as population growth [4,5].

Enhancing energy efficiency remains as a critical factor of sustainable energy strategies, offering numerous pathways to optimize the performance of systems. One promising avenue for achieving this objective is through waste heat recovery. This unused heat, which arises as a consequence in various production processes, often dissipates into the environment or water without being utilized. Consequently, effective management of waste energy has emerged as a pressing concern. Waste heat recovery finds applications across diverse sectors, including industrial production and residential building mechanical ventilation systems. Harnessing waste energy not only mitigates carbon dioxide emissions and environmental pollutants but also conserves primary fuel resources [6]. Thermoelectric generators (TEGs) enable direct conversion of waste heat into electricity, several studies in literature indicate that thermoelectric generators (TEG) are a favourable technology due to their compact structure and solid-state construction, and despite their low efficiency, TEGs are a particularly appealing option for energy generation and conversion [7,8].

TEG technology is based on the Seebeck effect and can be considered as solid-state energy generators operate without needing any moving parts. By utilising the Seebeck effect, TEGs can directly convert thermal energy to electrical one by exploiting the temperature difference between cold and hot sources [9,10]. Due to the lack of moving parts, the technology is compact and noise free, whilst being economically viable for most applications [11,12]. On the other hand, TEGs generally involve high upfront costs and are not particularly cost-effective which is a disadvantage [13]. The most common application for TEGs within the low-temperature waste heat recovery [14,15] from sources such as

* Corresponding author at: Heat Pipe and Thermal Management Research Group, College of Engineering, Design and Physical Sciences, Brunel University London, UB8 3PH, UK.
E-mail address: hussam.jouhara@brunel.ac.uk (H. Jouhara).

https://doi.org/10.1016/j.tsep.2024.102884
Received 4 June 2024; Received in revised form 20 August 2024; Accepted 5 September 2024
Available online 11 September 2024

solar energy [16], human body heat energy [17,18], cryogenic liquid cold energy [19], automobile exhaust waste heat [20], geothermal heat [21,22], and heat produced as a result of industrial production [23,24]. The flexibility and broad applicability allows the technology to be an extremely promising methods for low- and medium-temperature waste heat recovery [25,26].

To further understand the functionality and performance of TEGs, several computational and analytical models have been studied. For example, A method proposed for a system modelling of low-temperature gradient TEG with practical power conversion stage was introduced by Vostrikov et al. [27]. The method is built upon an analytical model that was updated and expanded to precisely replicate the input properties of actual DC-DC converters. The model operates based on the low temperature gradient approximation [28], incorporating Seebeck and Peltier effects while disregarding the Thomson effect and Joule heating. This simplification enables an accurate estimation of output power under steady-state ambient conditions, using simplified circuits. To enhance the model further and include DC-DC conversion, an expanded circuit diagram for a realistic TEG was also introduced. The TEG design characteristics, the surrounding environment, and the DC-DC converter's numerical model were used as the input to determine the output power. The research aimed to establish a reference point for researchers and manufacturers by validating the system modelling approach in real conditions through an experimental testbed. However, the original model's omission of the Thomson effect and Joule heating may restrict its relevance to TEG systems where these phenomena play a significant role in overall performance.

The geometric configurations of variable cross-section thermoelectric legs have received inadequate attention in the existing literature. Thus, Doraghi et al. [29] undertook a comprehensive investigation into the effect and performance of thermoelectric generators (TEGs) featuring novel leg geometries not previously explored. The study evaluated three leg geometries: the traditional Rectangular shape as a baseline, along with two new configurations—the Diamond shape and the Cone-based shape. Using COMSOL Multiphysics, the research conducted analyses of temperature distributions, voltage potential, and thermal stress for each proposed leg configuration, with each comprising two pairs of p and n materials. Furthermore, electrical analyses were conducted for TEG modules composed of 128 pairs of legs, examining two cases representing the lowest and highest voltage outputs for a double pair of legs. The findings revealed significant impacts of variable leg geometry on temperature distribution along the leg height. Notably, the Rectangular shape exhibited a smoother temperature distribution compared to the Cone and Diamond shapes. Regarding electric potential, the newly introduced Diamond shape demonstrated the highest voltage potential, while the Rectangular shape exhibited the lowest voltage potential. However, it's crucial to acknowledge that while the study provides valuable insights into the potential benefits of novel leg geometries, the new models introduced, namely the Diamond and Cone-based shapes, have yet to be fabricated. Additionally, experimental validation of these models has not been conducted. Therefore, the practical feasibility and real-world performance of these configurations remain untested.

Aymen and Hamdy [30] used ANSYS FLUENT to investigate a 3D TEG model. The premise of the study involved the study of recovering waste heat across the TEG module within a chimney wall. The study examines how the inlet flow velocity of hot gases and coolant air inside and outside the chimney affects heat transfer and the output power of the TEG. The findings indicate that optimal output power from the TEG modules occurs when the TEG is positioned at the inlet of the chimney wall where hot flow gases are at 600 K, and the cold junction is 300 K. However, the study focuses on a specific three-dimensional model of TEGs and its performance on a chimney wall, consequently, the applicability of the findings to different TEG setups or applications may be restricted.

Doraghi et al. [31] investigated two TEG models based on previously documented data. These models encompassed two distinct designs, one comprising 4-leg pairs and the other featuring 49-leg pairs of p- and n-type composites derived from polypropylene melt mixed with single-walled carbon nanotubes. Utilizing COMSOL Multiphysics software, the models were developed and subsequently validated against laboratory measurements. The TEG configurations involved 4 and 49 pairs of p- and n-type material strips, respectively. Upon comparing computational results with experimental data, it was observed that the relative error for the 4-leg pair model stood at approximately 8.6 %. However, for the 49-leg pair model, the discrepancy soared to 37 %. This disparity arose from the researchers' utilization of constant values for thermoelectric properties such as Seebeck coefficient, electrical conductivity, and thermal conductivity during simulation, despite the well-known temperature dependency of these properties. This study serves as a poignant reminder of the criticality of incorporating time-dependent property values in simulations to achieve heightened precision in thermoelectric research. By neglecting the temperature dependency of thermoelectric properties, the computational models fail to accurately capture the dynamic behaviour of thermoelectric phenomena. Thus, integrating time-dependent property values emerges as an imperative step toward enhancing the fidelity and reliability of thermoelectric device modelling and analysis.

In a separate study, the same researchers investigated a novel polymer nanocomposite-based TEG for waste heat recovery for aeronautical applications [32]. The study focused on assessing the TEG's performance under varied temperature gradients, showcasing promising outcomes for aeronautical applications. The TEG module, comprising four sections, each containing 17p-n strips, is fabricated from aerospace-grade polycarbonate, measuring 50 * 1 * 0.3 mm in dimensions. During the laboratory phase, the TEG undergoes comprehensive evaluation through a sequence of experiments. Temperature gradients, spanning from −15 °C to 55 °C, replicate scenarios encountered during ascent and descent phases of flight. The observed voltage outputs ranged from 67 mV to 116 mV, the results indicated the potential suitability of polymer-based TEGs for aviation applications, for instance. Specifically, temperature gradients ranging from 40 °C to 70 °C, simulating atmospheric and wing leading edge skin conditions, are applied across four experimental runs. Model validation established substantial agreement between computational predictions and experimental findings. Simulations conducted across varying temperature ranges offer valuable insights into the TEG's performance variations. Key discoveries include temperature distribution patterns, electric potential outputs under different circuit conditions, and a comprehensive analysis of fluid flow within a controlled thermal environment. However, the study faces limitations due to the inherent difficulties in producing polymer nanocomposite-based TEGs, alongside their lower efficiency compared to conventional counterparts. The intricate fabrication process of these TEGs presents a substantial obstacle, potentially hindering their scalability and real-world application.

Ding et al. [33] evaluated different fluid-thermal-electric multiphysics modelling methods for TEGs. The research introduces a new computational model for predicting the efficiency of TEG systems used for fluid waste heat recovery, taking into account the multiphysics coupling effects of fluid, thermal, and electric fields. The study noted that COMSOL coupled solver is the most reasonable approach to solving the fluid-thermal-electric multiphysics model. Moreover, the findings reveal that the output power projected by the COMSOL separate solver is notably lower (by 8.52 %) compared to that projected by the COMSOL coupled solver, primarily because parasitic heat effects are disregarded. Through experimental validation, it is demonstrated that the fluid-thermal-electric multiphysics model, solved by the COMSOL coupled solver, displays the smallest output power deviation (2.81 %) when compared to the ANSYS model.

Despite TEGs' immense potential for powering low-power systems, the poor conversion efficiency has emerged as TEGs' main disadvantage. To address this issue, modelling the thermoelectric conversion

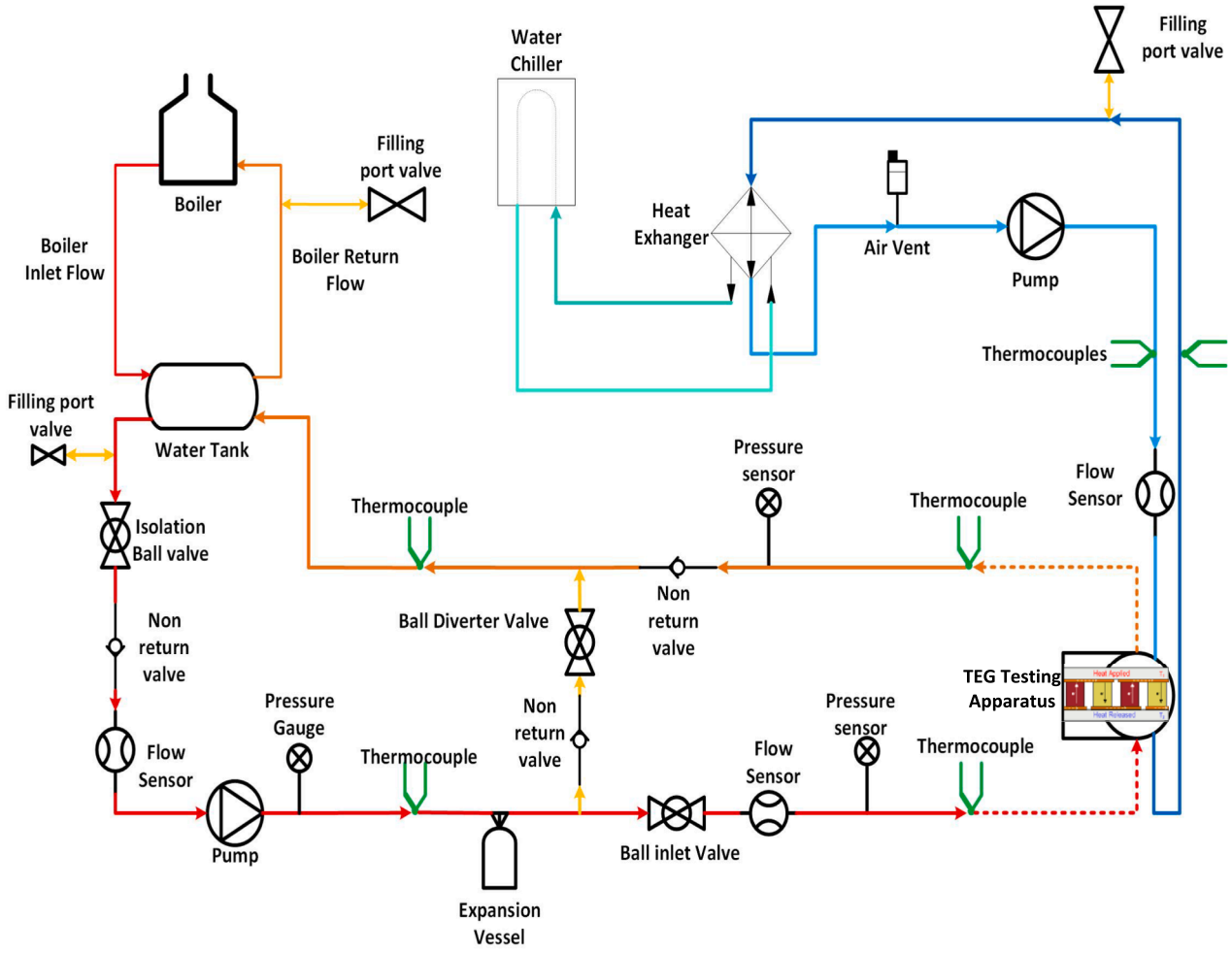

Fig. 1. Piping and Instrument diagram for the test rig.

characteristics is required, such as utilising an analytical model to assess how the thermoelectric conversion system is affected by thermal resistance and boundary conditions [34]. The effect of the maximum power and thermoelectric conversion efficiency, as well as a solution to decrease the system's heat loss, may all be studied by creating the thermoelectric system's parameter model and heat transfer network [35].

Minghui et al. [36], conducted a study experimentally investigating TEGs with varying amount of modules for waste heat recovery applications. ', The study investigated, the effects of the heat source flow, temperature, and number of thermoelectric modules on the thermoelectric properties, resistance, and power consumption of the generator. During the experiment, it was noted that the air flow and temperature are important aspects that influence the thermoelectric performance of the system and increasing these parameters improve output productivity.

Hewawasam et al. [37], conducted a study to understand the possibility of integrating the TEG to the muffler of an automotive exhaust, without interrupting the functionality of the muffler to recover the waste heat of the engine exhaust system. It was noted that TEG power generation decreases as coolant temperature rises.

Based on experiments and the multiphysics simulation modelling, Xuejin et al. [38] presented a size-enhanced TEG system with frustum-shaped thermoelectric legs in order to address the issues of low output electrical performance and energy conversion efficiency. The proposed model showed a 96 % increase in the TEG power output in comparison to the conventional rectangular model.

Whilst numerous investigations have explored the effectiveness of various thermoelectric systems, this study uniquely provides a comprehensive 3-dimensional computational analysis of TEGs using COMSOL Multiphysics 6.0. Unlike previous studies that often rely on simplified or 2-dimensional models, this research employs a fully 3D approach to capture the complex interactions within the TEG system more accurately. The integration of both thermal and electrical models in this 3D framework allows for a more precise analysis of temperature distribution, electrical output, and system efficiency across different operating conditions. Additionally, this study conducts a detailed examination of the relationship between internal and external load resistances and their impact on system efficiency, providing deeper insights into optimizing TEG performance. What sets this study apart is the rigorous experimental validation of the computational model, ensuring that the simulations closely mirror real-world performance. This high level of accuracy enhances the reliability of the findings and establishes a robust framework for future studies in thermoelectric energy conversion. Through these systematic simulations and thorough experimental comparisons, the research contributes valuable insights for advancing the application of TEGs in harnessing low-grade heat for electricity generation.

2. Experimental apparatus

A test rig was constructed and subjected to experimental testing, where aMAS15 – Elnur electric boiler was chosen as the primary heat source. This electric boiler played a pivotal role in generating hot water

Fig. 2. Aluminium extrusion plate.

Table 1
Heat exchanger tank specification.

Capacity	Orientation	Coils	Length	Width	Height	Weight
20 L	Horizontal	Single	800 mm	240 mm	245 mm	10 kg

which forms a part of a closed circuit with the heat exchanger.

This closed-loop circuit was designed, with attention to insulation and control mechanisms to maintain the temperature of the water within the desired operational range. A detailed Piping and Instrument Diagram (P&ID) as depicted in Fig. 1, outlines the specific arrangement of components within this circuit.

In tandem, in addtion, further circuit were generated consisting of a pump to facilitate the movement of hot water from the heat exchanger tank to the TEG. To optimize the heat transfer from the water to the TEG, an aluminium manifold was employed. This manifold served as an effective conduit, ensuring efficient heat conduction and promoting the overall performance of the experimental setup.

The manifold, a critical component of the system, is composed of an aluminium extrusion plate measuring 450 × 184 mm with a thickness of 10 mm. Two cylindrical connecting ports, designated for water inlet and outlet, are positioned on top of the manifold. Internally, the manifold features channels arranged in four passes, with each pass comprising four parallel channels, as illustrated in Fig. 2. This intricate internal structure enhances the heat exchange efficiency between the water and the TEG.

To provide a comprehensive understanding of the experimental apparatus, specific details regarding the heat exchanger tank are outlined in Table 1. This table includes key specifications such as material composition, dimensions, and capacity, offering a comprehensive overview of the primary vessel within the test rig.

Furthermore, a cooling system was incorporated to stabilize the temperature of the heat sink. A chiller, set at 5 °C, was employed in conjunction with Hexid A4 Heat Transfer Fluid, characterized by a temperature range of −15 °C to +90 °C. The chiller operated in a closed circuit, connected to a heat exchanger. This heat exchanger, in turn, was integrated into another circuit linked to the heat sink of the TEG. This comprehensive cooling system was imperative to ensure the stability of the heat sink temperature, providing a controlled environment for accurate experimentation.

To mitigate the risk of air interference with the flow sensor readings, an air vent was deliberately incorporated included into in the system. By doing so, the air vent served the essential purpose of removing air from the closed water circuit, safeguarding the accuracy of flow sensor readings. The air vent's placement was optimised by placing it at the highest point of the water loop. This was done to minimis the likelihood of air pockets within the system, thereby enhancing the precision of the experimental data.

Throughout the experimental procedure, a meticulous approach to data collection (i.e., using National Instrument datalogger) was maintained. Parameters such as temperature, pressure, and flow rate were systematically recorded at various points within both the heat source and heat sink of the TEG. The controlled variables (i.e., heat source and heat sink temperatures), were carefully monitored during testing., ensured consistency and reliability of the experimental outcomes. Safety precautions were also implemented to address potential hazards, including emergency shutdown procedures for immediate intervention if necessary.

2.1. Thermoelectric fitting

To enhance the voltage potential and power output, two Thermoelectric Generator (TEG) modules were used in the experimental setup. This integration of dual TEG modules aims to maximise the energy conversion efficiency and overall performance of the system. Ensuring proper thermal connection of a thermoelectric module is absolutely essential for its effective operation within a system. These modules depend on the efficient transfer of heat through them to function optimally. Any factors that hinder this thermal transfer, such as the introduction of additional thermal resistance or obstacles, can lead to

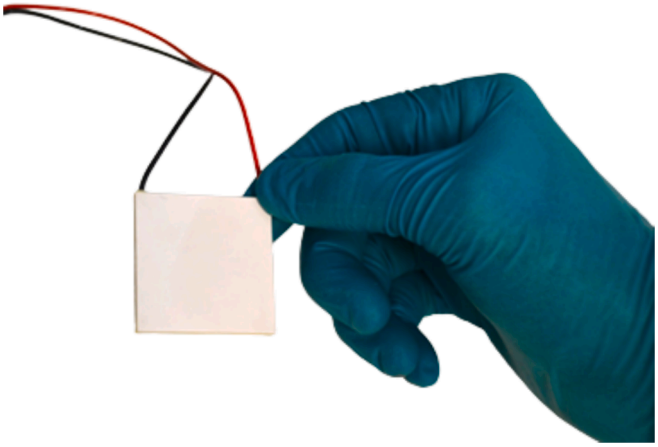

Fig. 3. TEG module used for the experiment.

significant decreases in performance. In other words, the successful functioning of thermoelectric modules hinges on the seamless flow of heat, and any hindrance to this process can significantly impact their efficiency.

The initial step involves the proper orientation of the module to suit the specific application. This is a critical consideration as the maximum temperature specifications can frequently vary for each side of the module. As shown in Fig. 3 GM200-127-28-12 [39] thermoelectric generator module was employed for this experiment.

2.1.1. Determining hot and cold side

To determine the hot and cold sides, the procedure involved operating the thermoelectric module as a generator. Wires were directly connected to the corresponding-coloured leads of a voltmeter, and the thermoelectric module was positioned on a surface (expected to be at or below room temperature), such as a tabletop. A hand was then placed on the side of the module facing upwards, effectively simulating a temperature differential, with the hand being warmer than the tabletop surface. If the voltmeter displayed a slight positive voltage, it indicated that the hot side was the one in contact with the hand. Conversely, if the voltmeter showed a minor negative voltage, it would meant that the cold side was the one in contact with the hand.

2.1.2. Thermal grease

In operating conditions below 100 °C, as was the case for this experiment, it is common practice to utilize thermal greases as the interface material. Due to their high thermal conductivity properties and their capacity to fill in any imperfections at the interface. Such interface materials are frequently employed in cooling modules and on the cold side of generator modules to facilitate effective thermal coupling with a heat exchanger. The application of thermal grease involves spreading it onto the ceramic surface of the modules, a process that serves to diminish the impact of any air gap resulting from surface irregularities, thereby augmenting the surface contact area.

In order to apply thermal grease, the following procedure was followed:

Step 1: To clean the surface from debris and grease.
Step 2: Applied a pea-sized quantity of thermal grease to the centre of the ceramic surface on the module.
Step 3: Use a plastic card or blade to evenly distribute the grease across the ceramic surface, ensuring comprehensive coverage with no areas left uncovered.
Step 4: Conducted a final scraping to guarantee uniform coverage and remove any excess grease to the greatest extent possible.

Silicone grease with a thermal conductivity of 5.2 (W/m.K) was employed to achieve optimal performance.

2.1.3. Bonding method

The last phase in integrating a thermoelectric module into the system is the clamping and system assembly stage. It is crucial to achieve adequate clamping and preserve thermal isolation for the surrounding components to attain the highest possible performance from the device. Inadequate clamping of a thermoelectric module can result in performance reductions of approximately 20 % [40]. The thermoelectric module is positioned between the heat sinks on the hot side and cold side, establishing full contact with both. Compression is exerted on the module using bolts evenly spaced along the module's edge. It is essential to tighten all bolts at the same rate until they achieve the optimum clamping torque. These bolts are thermally insulated, serving to prevent thermal contact between the hot and cold sides, thereby minimizing parasitic losses in the system.

Thermoelectric modules necessitate a clamping load within the range of 0.5–1.2 MPa. To attain this clamping load within a system, bolts are the most frequently employed fasteners, and they are tightened to a precise torque. To compute the required torque for achieving the desired clamping force, Formula 1 was utilised [40]:

$$T = \frac{C^*D^*P^*A}{N} \quad (1)$$

where:

C = Torque coefficient.
P = Compression Pressure (Pa).
N = Number of screws.
D = Nominal bolt size (mm).
A = Total module footprint area (m^2).
T = Torque per screw (N.m).

In this specific system, two M8 bolts were employed to clamp a 40 mm × 40 mm module. These bolts were used without lubrication, and their torque coefficient (C) is estimated to be approximately 0.2. The nominal bolt size 'D' is 8.2 mm, and the target clamping load is 1.2 MPa. Therefore, the torque per bolt is calculated as 1.57 N.m.

2.1.4. TEG module integration and heat transfer mechanism

The experiment incorporated the placement of two TEG modules onto an aluminium manifold. The aluminium manifold served as the primary medium for transferring heat generated by the electric boiler to the TEG modules. To minimize heat loss to the surroundings and enhance the interaction with the TEG modules, insulative measures were employed.

In Fig. 4-A, the aluminium manifold is seen enveloped in insulation and secured with silver tape, it should be mentioned that the thermal conductivity of the insulation is 0.69 W/m.K [41]. This insulation, applied to the manifold, was designed to create a thermal barrier, preventing undesired heat exchange with the environment.

Before the installation of the TEG modules, a layer of silicone thermal grease was carefully applied to the interface between the aluminium manifold (Fig. 4-B) representing the heat source, and the TEG modules.

The experimental setup involved the circulation of high-temperature water through the manifold. The water entered from one end, absorbing heat from the aluminium manifold, and subsequently transferred this thermal energy to the integrated TEG modules. Upon interacting with the TEG modules, the water exited the manifold at a slightly lower temperature. This design, crafted to facilitate effective heat transfer, ensured that the TEG modules received a consistent and controlled thermal input.

The integration of TEG modules into the experimental setup played a pivotal role in harnessing the temperature gradient created by the heated water flowing through the manifold while maintaining the heat

Fig. 4. A) Insulated manifold before placing the TEG. B) Insulated manifold after placing the TEG and the thermal grease C) Top view of the manifold D) Bottom view of the manifold.

sink at the desired low temperature.

Following the insulation of the aluminium manifold and the application of silicone thermal grease, the next crucial step in the experimental setup involved the assembly of the TEG modules. The top and bottom sections of the manifold, each housing TEG modules, were clamped together to form a cohesive unit as shown in Fig. 4-C and D.

To capture the dynamic performance of the experimental system, a comprehensive instrumentation setup was implemented. K-type thermocouples were attached to various points within the system. These thermocouples served as temperature sensors and facilitated data acquisition through the Dataweb-4016. Electrical readings were particularly recorded using the IDM 98IV Digital Multimeter, known for its impressive 0.1 % accuracy.

Once all components were securely attached, the system commenced operation. The water connection point, a critical juncture in the experimental setup, featured an Omega® Turbine Flow Sensor FTB371-G and a valve for regulating the water flow rate. This configuration provided control over the water flow, a key factor influencing the heat transfer

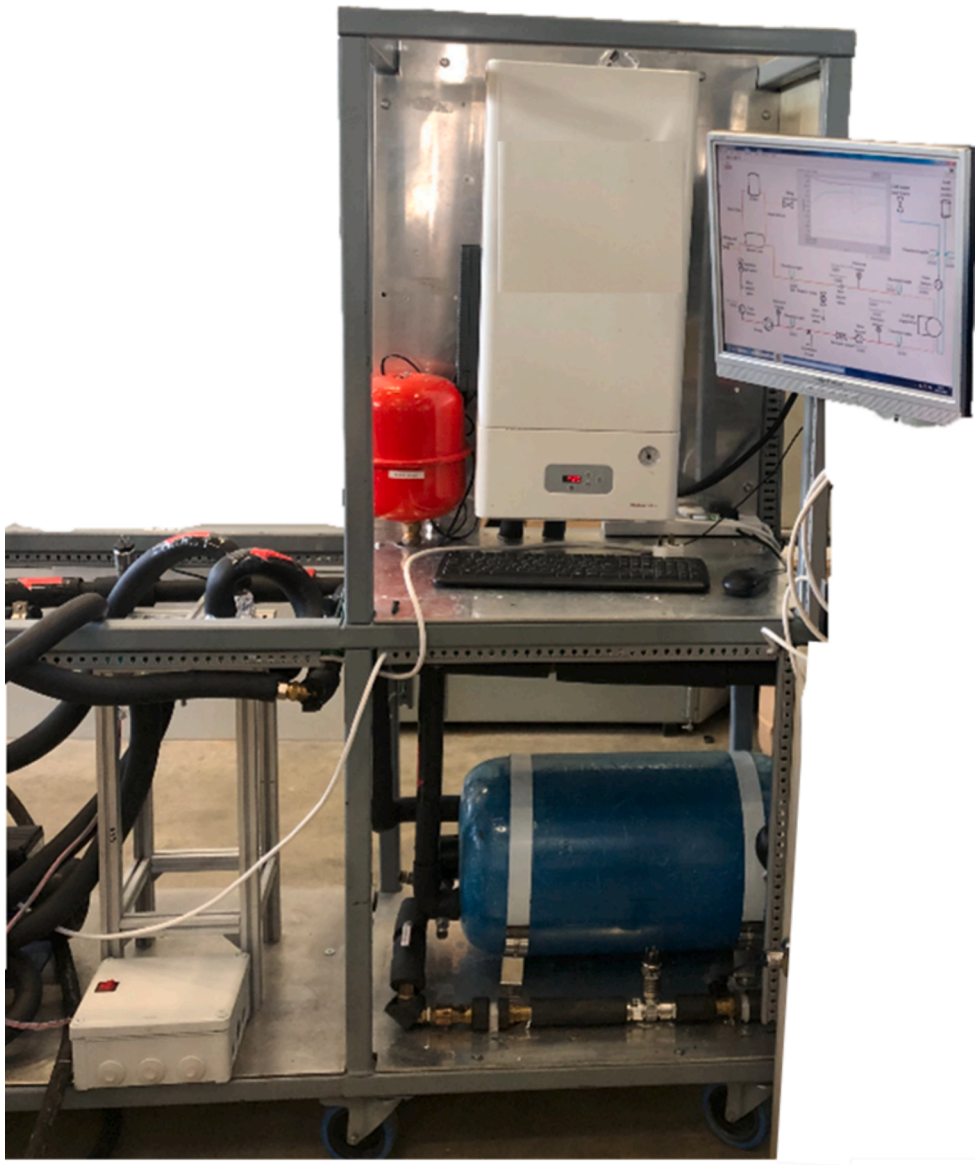

Fig. 5. TEG test rig in operation.

within the system.

Positioned at the rear of the test rig, a network of thermocouples embedded within the system was interconnected to a data logger. This data logger featured two thermocouple modules (NI-9213) and interfaced with a computer for real-time data visualization and recording. LabVIEW software served as the interface, offering a user-friendly platform for monitoring and analysing the experimentally obtained data.

To exert precise control over the power supply to the system, a dedicated control box was constructed. This control box incorporated temperature controllers designed exclusively for safety measures, working in tandem with a power controller.

It must be highlighted that to ensure accurate measurement of the temperature difference across the TEG, thermocouples were positioned at key locations within the system. For the heat source, thermocouples were attached just before the hot water inlet into the TEG and immediately after the hot water outlet of the TEG. This placement was designed to capture the precise temperature differential as the water flowed through the TEG. Similarly, for the heat sink, thermocouples were placed before the cold-water inlet and after the cold water outlet, allowing for an accurate measurement of the temperature difference on the cooling side. These specific placements ensured that the temperature readings directly reflected the conditions impacting the TEG's performance, thereby enhancing the accuracy of the experimental data.

The overall arrangement of the experimental test bench, as illustrated in Fig. 5, provides a visual representation of the TEGs in action during the testing phase.

3. Computational simulation; thermal-electric multiphysics models of the thermoelectric generator system

3.1. Model

Based on TEG GM200-127-28-12, a TEG model made of 127 pairs was designed. The dimension of the TEG is 64 × 64 × 4 mm. This investigation relied on COMSOL Multiphysics to model and simulate the intricate physical processes within TEGs. COMSOL Multiphysics was chosen because of its robust suite of tools tailored for multifaceted simulations, offering a versatile platform that extends beyond generic applications. COMSOL has the ability to accommodate multiple coupled physics, essential for accurately representing real-world systems [42]. Specifically, the analysis integrated Heat Transfer in Solids, Electric

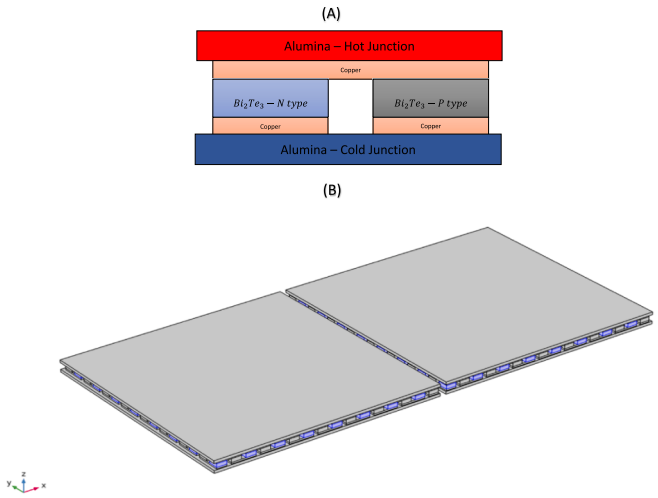

Fig. 6. Model used for COMSOL simulation A) One pair of a TEG with its materials. B) Two full TEG modules.

Current, and Electric Circuit, reflecting the intricate coupling inherent in TEGs' operating environment [43].

COMSOL's deployment of advanced numerical techniques is paramount in our pursuit of accurate simulations. By effectively handling nonlinear, time-dependent, and coupled physics issues, COMSOL ensures dependable results that capture the dynamic behaviour of TEGs, this commitment to accuracy is essential for deriving meaningful insights into TEG performance across varying conditions. Visualization tools within COMSOL empower researchers to intuitively understand and interpret simulation results. Graphical representation in 2D and 3D, animations, and other visualization techniques facilitate a comprehensive analysis of TEGs' thermal and electrical behaviour, this visual feedback enriches understanding and aids in drawing meaningful conclusions from simulations [44].

Additionally, COMSOL could be used for optimization studies to determine the optimal design parameters for a particular situation. This can result in better product designs as well as cost reductions in engineering applications [45,46].

Overall, COMSOL Multiphysics allows the researchers to create models through describing the phenomena, structure the geometry, generating the mesh and then solving and analysing the results. As for this simulation, two TEGs were designed and connected through copper wire. Fig. 6 indicates the TEGs used for this simulation.

A model component is a core aspect of the computational design that contains a geometry with its related physics interface, mesh, variables, and other local specifications. The component node describes the name space for each part of the model that is defined in the model component.

3.1.1. TEG Fundamental equations

To establish a theoretical framework for analysing the thermoelectric generator (TEG) performance, it is essential to define the key equations that govern the system's behaviour. The relationship between the electrical potential of a TEG and its temperature difference is described by Eq. (2).

$$\Delta V = S^*\Delta T \tag{2}$$

where S is the Seebeck coefficient.

Additionally, the power output generated by the TEG is quantified using Eq. (3).

$$P_{out} = V^*I \tag{3}$$

Finally, the efficiency of the TEG, considering both the heat input and electrical output, is detailed in Eqs. (4) and (5).

$$\eta = \frac{P_{out}(w)}{Q_{in}(w)} \tag{4}$$

where:

$$Q_{in} = Q_h - Q_c \tag{5}$$

where $Q_h(w)$ is the heat transfer from the heat source, and $Q_c(w)$ is the heat transfer to the heat sink.

These foundational equations provide the necessary mathematical basis for the subsequent computational and experimental analyses presented in this study. For a more in-depth analysis of these equations and their derivations, readers are referred to [29].

3.2. Boundary condition

Heat transfer in solids, electrical currents and electrical circuit interfaces were used in this simulation to describe the Thermoelectric phenomenon. Thermal insulation is a default boundary condition for all heat transfer interfaces. Using this boundary condition will prevent any heat flux throughout the boundary. Moreover, within the heat transfer in solids interface, two temperature nodes (hot and cold junctions) were applied on the top and bottom surfaces respectively to act as a heat source and heat sink.

Convective heating is a frequent boundary condition for modelling heat transfer, in which a fluid cools or warms a surface by either natural or forced convection. In theory, the heat flux is defined by Eq. (6).

$$q_0 = h(T_{ext} - T) \tag{6}$$

where $q_0(\frac{w}{m^2})$ is the heat flux, h is a heat transfer coefficient and $T_{ext}(K)$ the temperature of the environment, and T is the boundary temperature.

The heat transfers from the heat source to the heat sink of the thermoelectric module according to conduction Fourier's law [47]:

$$q_x = -KA\frac{dT}{dX} \tag{7}$$

where q_x is the heat transfer rate (w), K is the thermal conductivity of the material $\left(\frac{W}{m.C^\circ}\right)$, $A(m^2)$ is the area of the surface the heat is being transferred, $\frac{dT}{dX}\left(\frac{C^\circ}{m}\right)$ is the temperature gradient in the direction of heat transfer. Fig. 7 shows the heat transfer rate of the TEG.

In the electrical currents interface, COMSOL automatically applies to

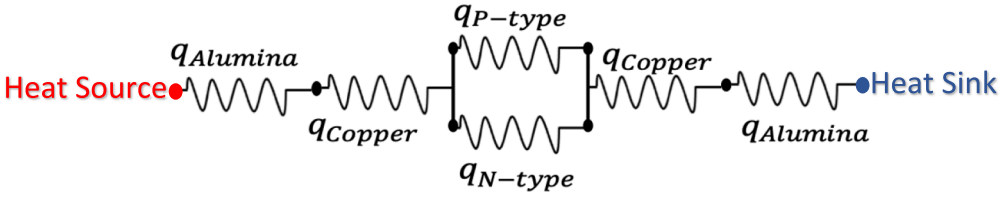

Fig. 7. Heat transfer rate in a TEG.

Table 2
Material properties of the TEG system.

Component	Material	Density: ρ (Kg. m^{-3})	k (W/ (m. k))	S (V/ K)	σ (S/m)	Heat capacity at constant pressure: Cp [J/(kg*K)]
Ceramic substate	Alumina	3900	–	–	–	900
P-type material	Bi_2Te_3	7700	KP (T)	SP (T)	$\sigma_P(T)$	154
N-type material	Bi_2Te_3	7700	KN (T)	SN (T)	$\sigma_N(T)$	154
Electrode connector	Copper	8960	–	–	$5.998*10^7$	385

the current conservation node. This node provides the continuity equation for the electric conductivity as well as the constitutive relation and the relative permittivity for displacement current. Another default node in the interface is the electric insulation. This node stops the electric current flows into the boundary. An initial values node delivers an initial value for the electric potential. To implement the zero potential $(V = 0)$ as a boundary condition, a ground node was added. Floating Potential node is the final boundary which was added to the electrical current interface. This node enables the user to calculate the overall electrical potential. The analysis was conducted under steady-state conditions.

3.3. Materials

The materials used in the simulation are listed below in Table 2, while Table 3 provides correlations to obtain the accurate value for the temperature dependant materials. These correlations were provided by the manufacturer [40].

3.4. Mesh study

In order to obtain a precise result in the lowest amount of time, a suitable mesh must be generated. To optimise computational power whilst obtaining the most accurate result, a mesh study was conducted. Effective mesh generation in COMSOL Multiphysics involves considering various factors, all of which can be explored using the software's diverse features and functionalities. For instance, users have the option to choose between different mesh sequence types, enabling either automated meshing or custom mesh creation. This customization grants control over critical parameters such as the order of operations in the meshing sequence, the types of elements utilised, and the size and

Table 3
Thermoelectric properties of the Bi_2Te_3-based material.

Name	Seebeck coefficient S (V/K)	Thermal conductivity k (W/ (m.k))	Electrical conductivity σ (S/m)
P-type material	$S_P(T) = (-0.003638095*T^2 + 2.74380952*T - 296.214286)*10^{-6}$	$K_P(T) = (0.0000361558*T^2 - 0.026351342*T + 6.22162)$	$\sigma_P(T) = (0.015601732*T^2 - 15.708052*T + 4466.38095)*10^2$
N-type material	$S_N(T) = (0.001530736*T^2 - 1.08058874*T - 28.338095)*10^{-6}$	$K_N(T) = (0.0000334545*T^2 - 0.023350303*T + 5.606333)$	$\sigma_N(T) = (0.01057143*T^2 - 10.16048*T + 3113.71429)*10^2$

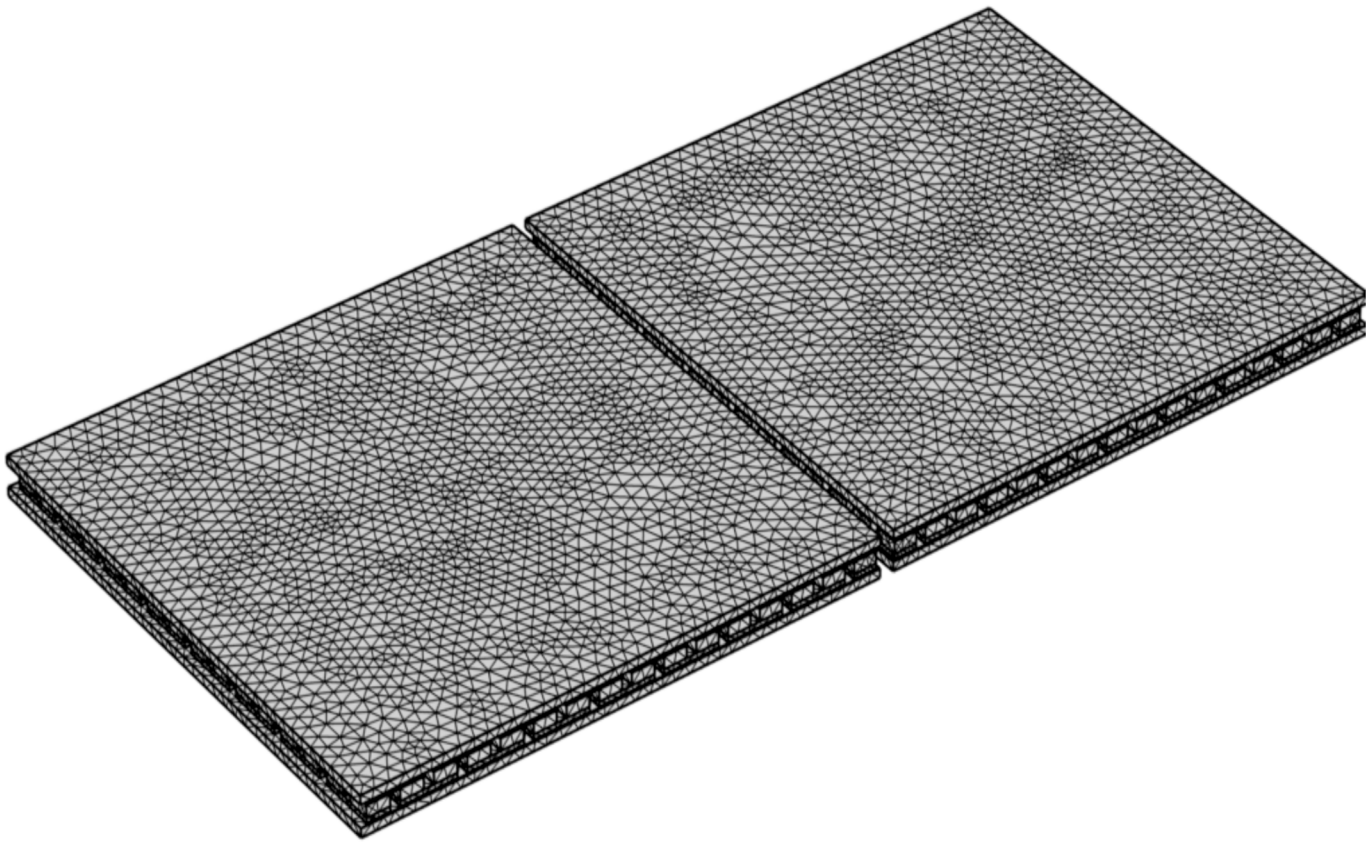

Fig. 8. Free tetrahedral mesh.

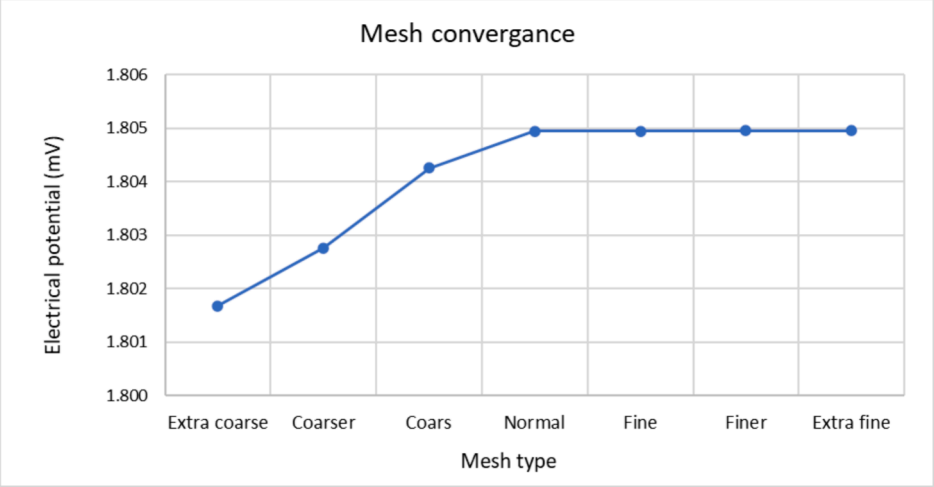

Fig. 9. Variation of TEG electrical potential with different mesh type.

Table 4
Mesh type and number of elements used for the simulation.

Model	Normal
Number of elements	123,506
Minimum element quality	0.1501
Average element quality	0.6195
Element volume ratio	0.02208
Mesh volume	24440.0 mm^3

Table 5
Estimated measurement uncertainties.

Parameter	Symbol	Measurement Uncertainty
Flow rate Uncertainty	$\delta_{\dot{m}}$	±0.05%**Averageflow*
Thermocouple Uncertainty	δ_{Tc}	1.45 K

Table 6
Maximum errors associated with the experimental heat transfer rates.

Trial	Temperature difference	Heat Transfer Rate – $Q_h(W)$	Maximum error $\delta_{\dot{Q}}$	maximum relative error $\delta_{\dot{Q}}/Q_h$%
1	24.36	178.53	2.054	1.15 %
2	33.82	230.82	2.054	0.89 %
3	43.84	280.56	2.054	0.73 %
4	53.96	341.18	2.054	0.60 %
5	63.45	390.79	2.054	0.52 %
6	67.90	428.22	2.054	0.48 %

Trial	Temperature difference	Heat Transfer Rate –$Q_c(W)$	Maximum error $\delta_{\dot{Q}}$	maximum relative error $\delta_{\dot{Q}}/Q_c$%
1	24.36	178.53	2.054	1.67 %
2	33.82	230.82	2.054	1.26 %
3	43.84	280.56	2.054	1.00 %
4	53.96	341.18	2.054	0.82 %
5	63.45	390.79	2.054	0.71 %
6	67.90	428.22	2.054	0.66 %

distribution of elements [44]. These considerations are pivotal not only for accurately resolving the model geometry but also for optimizing efficiency. It is worth noting that the mesh employed in COMSOL simulations significantly influences modelling requirements and constitutes one of the most memory-intensive steps in setting up and solving the finite element problem [48]. In this model, various meshing types were tested, and the appropriate mesh (Free Tetrahedral) was selected accordingly as shown in Fig. 8.

Fig. 9 illustrates the analysis of electric potential variation from the TEG model across different mesh types. The graph reveals that a plateau of nearly constant electrical potential is reached after a finite number of elements, hence, Normal Free Tetrahedral mesh to fulfil convergence criteria.

This choice is considered crucial in the modelling process to ensure the acquisition of precise results efficiently, without compromising solution accuracy. Table 4 indicate more details of the mesh.

4. Error analysis

Before presenting the results and discussion, it is crucial to outline the data reduction techniques and error propagation methods employed in this study. These processes were essential for ensuring the accuracy and reliability of the experimental data. Targeted data reduction techniques were applied to precisely calculate the heat transfer rates and efficiency metrics, which are central to the subsequent analysis. Following data reduction, the measurement uncertainties were quantified using detailed error propagation techniques. These methods, described in the following sections, played a significant role in shaping the interpretation of the experimental results.

4.1. Data reduction

In pursuit of characterizing the thermal performance of the thermoelectric generator, the initial raw dataset originating from thermocouples and the water flow rate is subjected to a process of reduction for the derivation of additional quantifiable parameters. The determination of the experimental heat transfer rate transiting through the system involves the utilization of water mass flow rate and temperature measurements at both the inlet and outlet points for both the hot and cold junctions of the TEG could be done via:

$$\dot{Q} = \dot{m}^* c_p^* (T_{out} - T_{in}) \tag{8}$$

where $\dot{Q}$ (W) is the heat transfer rate through the system, $\dot{m}$ (kg/s) is water flow rate in the manifold, c_p $\left(\frac{J}{kg.K}\right)$ is the specific heat capacity of water at constant pressure, T_{out} and T_{in} are the water outlet and inlet temperatures (K) respectively. Moreover, in order to deduce the efficiency, the heat transfer rate for both the hot $(\dot{Q}_h)$ and cold $(\dot{Q}_c)$ sides were calculated from Eq. (4).

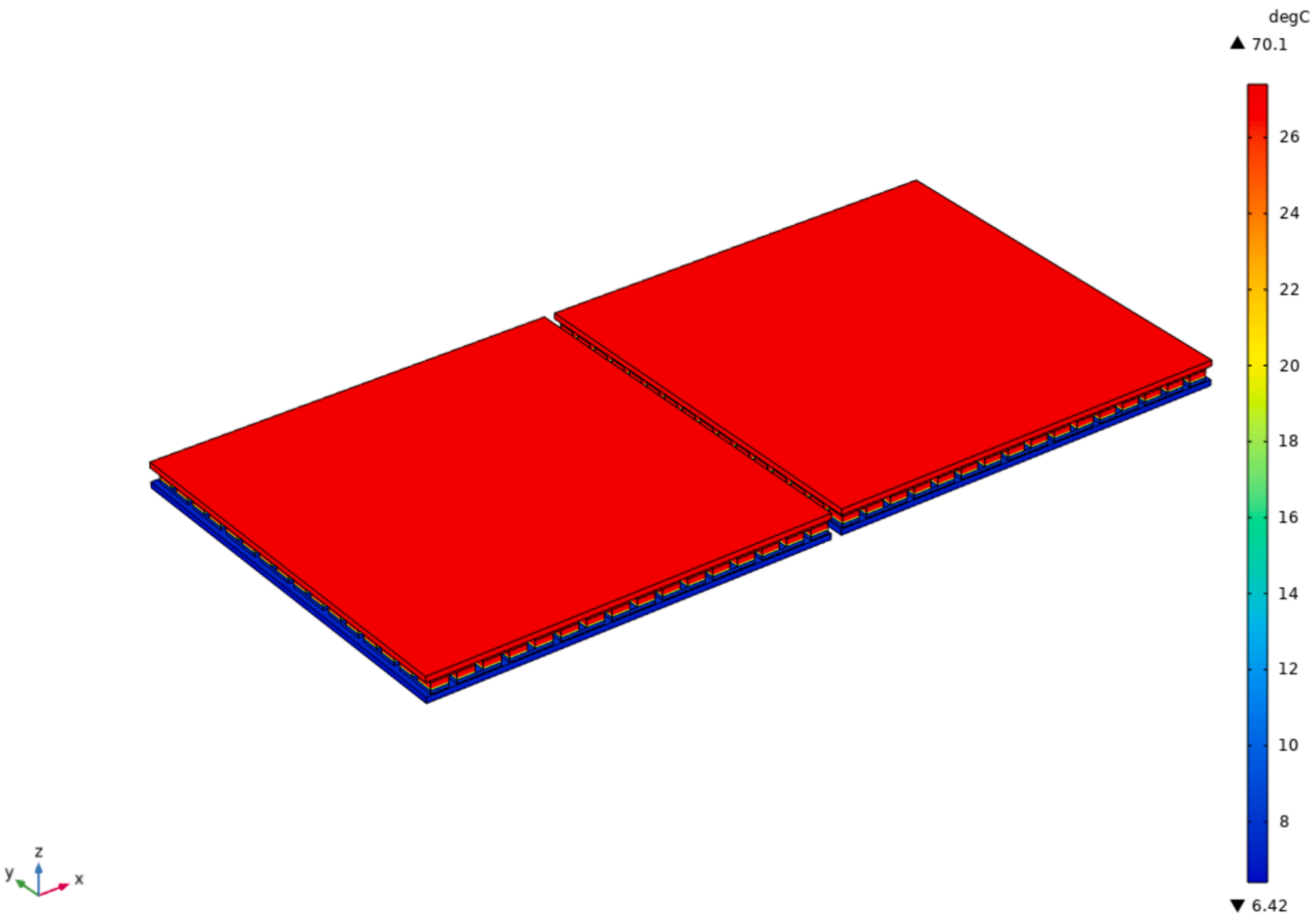

Fig. 10. Temperature distribution.

4.2. Error propagation and standard deviation

The precision of the experimental results was evaluated by assessing the propagation of measurement errors inherent in the data acquired from sensors. Two distinct strategies for error estimation were considered and subsequently compared. One approach involves the theoretical estimation of errors, encompassing the consideration of uncertainties originating from the sensors. This method entails a comprehensive analysis of error propagation within the framework of the data reduction equation. Alternatively, the assessment of experimental error involves examining the standard deviation among multiple experiments.

This methodology primarily estimates the scatter of data but may not detect systematic errors. Beginning with the measurement uncertainty, the temperature measurement error originating from the thermocouples was appraised through a series of 10 measurements conducted on 4 distinct K-type thermocouples immersed in both cold and boiling water environments. Moreover, the uncertainty associated with the water flow rate was stipulated by the manufacturer at ±0.05 %. The resulting estimated measurement uncertainties are detailed in Table 5.

The total uncertainty associated with the thermocouples was calculated from Eq. (5):

$$\Delta\boldsymbol{\delta}_{TC} = \sqrt{(\boldsymbol{\delta}\mathrm{TC}_{waterout})^2 + (\boldsymbol{\delta}\mathrm{TC}_{waterin})^2} = \sqrt{(1.45)^2 + (1.45)^2} = 2.05 \quad (5)$$

Using the estimated uncertainties in temperature and flow rate measurements, it is possible to calculate the absolute maximum uncertainty in assessing the heat transfer rate from the Eq. (6):

$$\text{While}: \quad \boldsymbol{\delta}_{\dot{Q}} = \sqrt{(\Delta\boldsymbol{\delta}_{TC})^2 + (\boldsymbol{\delta}\dot{\boldsymbol{m}})^2} = \sqrt{(2.05)^2 + (0.13)^2} = 2.054 \quad (6)$$

The maximum errors related to the experimentally determined heat transfer rates are documented in Table 6. As indicated, the calculated error is exceedingly minimal and diminishes with increasing Q. It is essential to highlight that the errors associated with both systems exhibit similarity and follow a consistent trend in terms of relative error.

As can be seen, the experimental error diminishes as the heat transfer rate increases. This trend can be explained by the fact that higher heat transfer rates result in more significant temperature differences within the system. These increased temperature variations contribute to a reduction in the relative error associated with the temperature measurements obtained from the thermocouples.

4.3. Standard deviation, mean deviation and standard error

To determine the reliability of the results, the experiment must be repeated several times.

This iterative approach offers the opportunity to observe patterns and trends within the dataset, effectively mitigating the influence of anomalous errors. As anomalous errors tend to average out over multiple trials, the precision of the measurements is substantially improved. Averaging data from repeated experiments aids in deriving a more accurate estimation of the central tendency, notably the mean value, for each measured quantity.

Moreover, the repeated trials allow for a more comprehensive statistical analysis of the data. Calculating the mean and standard deviation across multiple experiments provides a quantitative measure of the spread or variability in the results, adding a layer of depth to the uncertainty assessment. It is crucial to conduct a thorough investigation of any anomalies within the dataset, as these instances may signify

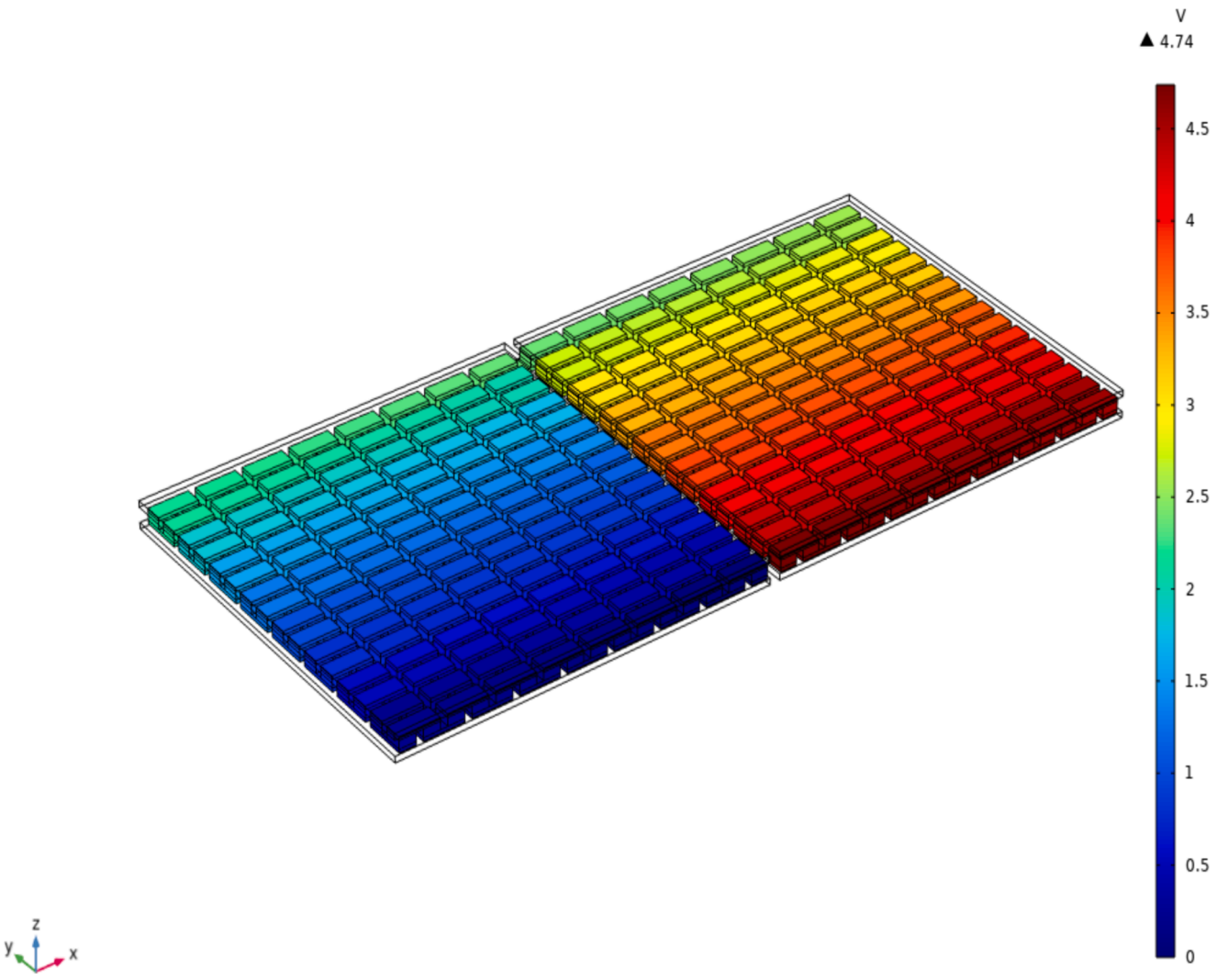

Fig. 11. Electrical distribution.

potential systematic errors or other issues that merit attention.

In the context of the uncertainty analysis for this research, statistical methods such as Standard Deviation (σ), Mean Deviation and Standard Error (SE) were employed to establish confidence intervals around the mean values. These intervals offer a range within which the researchers can express reasonable confidence that the true value lies. The robustness of the findings is further substantiated by comparing results from different trials, ensuring consistency and validating the reliability of the experimental setup.

Beyond enhancing precision and reliability, repeating the experiment also facilitates the identification and potential mitigation of systematic errors. If systematic errors are present, consistent biases across multiple trials become apparent, prompting a more targeted investigation into their root causes.

Mean Deviation

Trial	**Open Circuit Voltage**	**Closed Circuit Voltage − 1 O**	**Closed Circuit Voltage − 2 Ohms**
1	0.081	0.028	0.040
2	0.102	0.024	0.043
3	0.089	0.020	0.038
4	0.099	0.022	0.034
5	0.110	0.020	0.036
6	0.206	0.046	0.088

(*continued on next column*)

(*continued*)

Standard Deviation (σ)

Trial	**Open Circuit Voltage**	**Closed Circuit Voltage − 1 O**	**Closed Circuit Voltage − 2 Ohms**
1	0.104	0.041	0.057
2	0.117	0.032	0.050
3	0.103	0.028	0.050
4	0.109	0.031	0.045
5	0.125	0.028	0.054
6	0.220	0.053	0.097

Standard Error ($\boldsymbol{SE}$)

Trial	**Open Circuit Voltage**	**Closed Circuit Voltage − 1 O**	**Closed Circuit Voltage − 2 Ohms**
1	0.028	0.011	0.015
2	0.031	0.009	0.013
3	0.028	0.008	0.013
4	0.029	0.008	0.012
5	0.033	0.007	0.014
6	0.059	0.014	0.026

The low values observed for mean deviation, standard deviation, and standard error in the analysis of open circuit voltage, closed circuit voltage at 1 O, and closed-circuit voltage at 2 O indicate a tight clustering of data points around their respective means. This close alignment

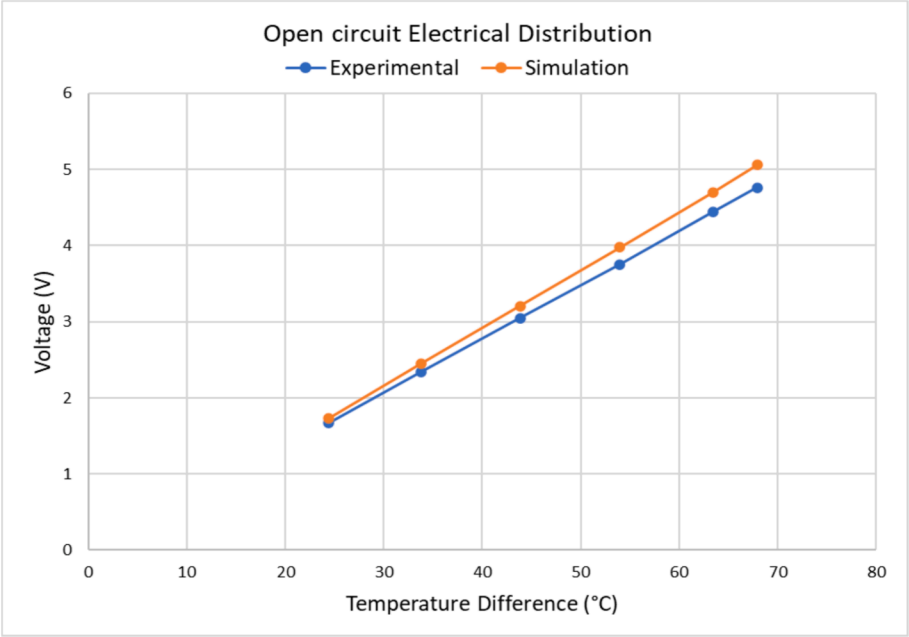

Fig. 12. Open circuit voltage potential computational simulation Vs experimental.

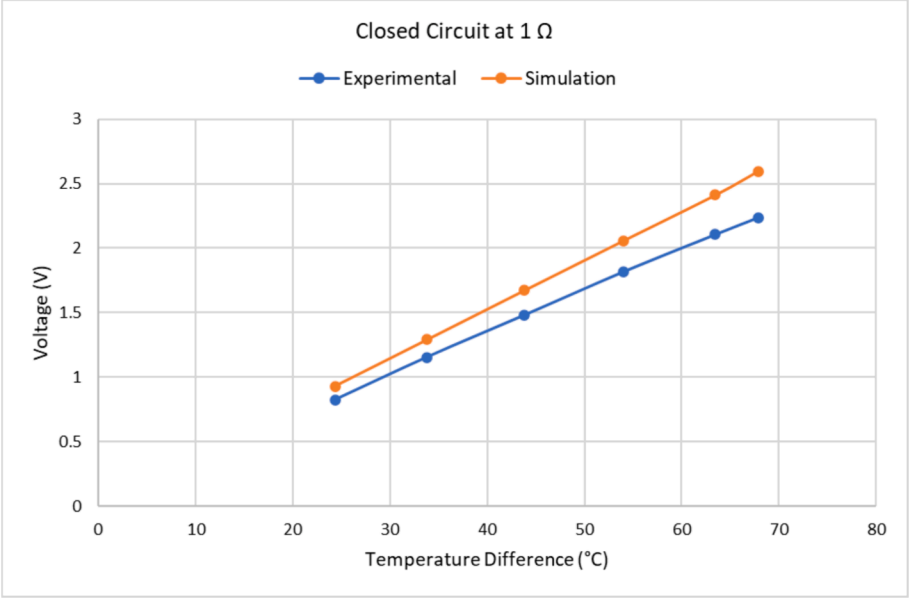

Fig. 13. Closed circuit voltage potential at 1 Ω; computational simulation Vs experimental.

suggests a notable level of consistency and uniformity in the experimental dataset.

5. Result and discussion

There are two ways to approach the system of equations that explain the result when using COMSOL Multiphysics to solve the model.

1. The fully coupled technique creates a single system of equations that, in a single iteration, simultaneously solves for all the unknowns and the couplings (the multiphysics effects).
2. The segregated technique, on the other hand, will not solve for all the unknowns at once. It breaks the problem into two or more segregated steps instead. Typically, each step represents a single physics, although even a single physics can be broken into stages, and one step can comprise numerous physics. Individual segregated steps are smaller than the entire system of equations created by the fully coupled method. Segregated steps are solved sequentially inside a single iteration, requiring less memory.

In many circumstances, especially with 3D models (i.e., this study), the COMSOL will automatically choose the segregated technique. The fully coupled method, on the other hand, is the default for most 2D models. These default settings have been chosen for their overall durability.

Overall, the thermoelectric generator made of 127 pairs of p-type and n-type was entirely modelled and its performance was comprehensively investigated through the steady-state Segregated Solver.

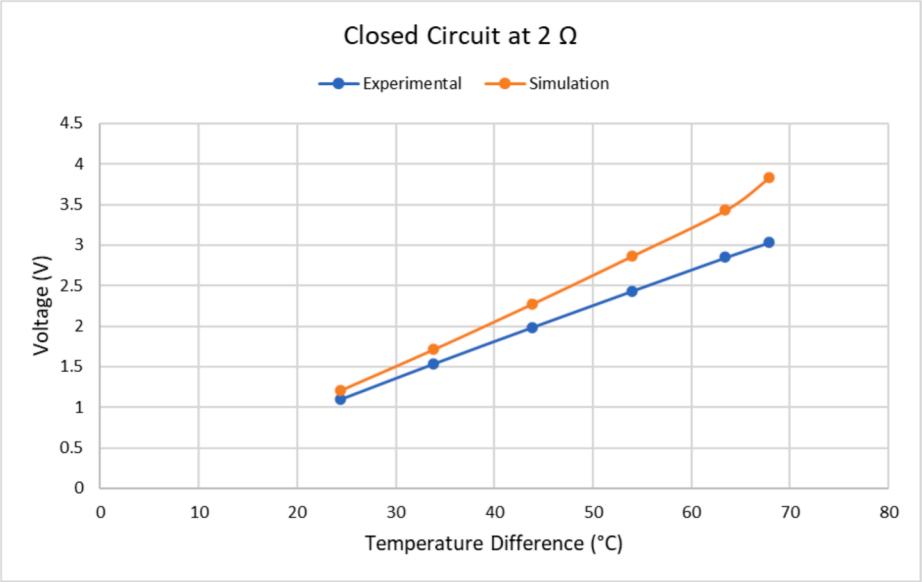

Fig. 14. Closed circuit voltage potential at 2 Ω; computational simulation Vs experimental.

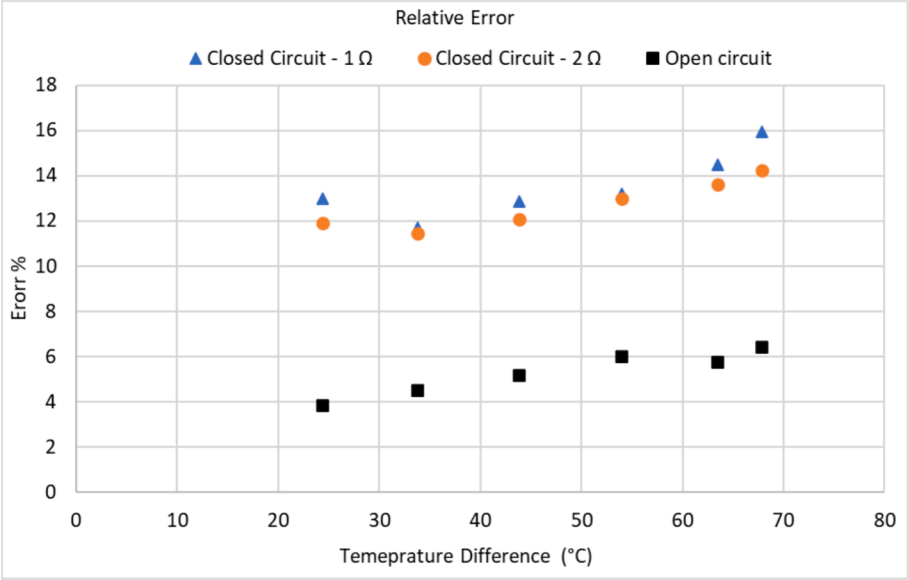

Fig. 15. Relative error associated with the voltage potential between the experimental Vs computational simulation.

5.1. Temperature distribution

In the simulation of TEGs, a parallel thermal connection configuration was employed. In this setup, a heat source, and a heat sink, were applied to the top and bottom of the TEG, respectively. For the purposes of this research, the heat sink was maintained at the same temperature as the average experimental heat sink temperature.

Contrastingly, the heat source was subjected to six distinct temperatures. The initial temperature was set at 30 °C, with subsequent increased increments of 10 °C, reaching temperatures of 40, 50, 60, 70, and finally 75 °C. This variation in heat source temperatures aimed to replicate the experimental boundary conditions observed in the physical experiment. Fig. 10 illustrates the temperature distribution observed when the heat source is set at 70 °C. This depiction offers insights into the thermal behaviour of the thermoelectric generator under specific operating conditions, aiding in the analysis and understanding of its performance at this particular temperature setting.

5.2. Electrical distribution and model validation

The electrical interconnection of thermoelectric elements is configured in series, resulting in a potential difference between the ground node and the floating potential node. In the simulation, the model was executed under both open Circuit and closed-circuit conditions. Specifically, for the closed-circuit scenario, the TEG was simulated with external loads of 1 Ω and 2 Ω. Fig. 11 provides insights into the electrical distribution when simulating at 75 °C, contributing further to the understanding of the electrical behaviour under varied temperature conditions.

Notably, it was observed that the electrical potential, both in open circuit and closed-circuit configurations, exhibited an upward trend with increasing temperature. This correlation is attributed to the direct relationship between the electrical potential of a TEG and its temperature difference.

For visual representation, Fig. 12 illustrates the electrical potential

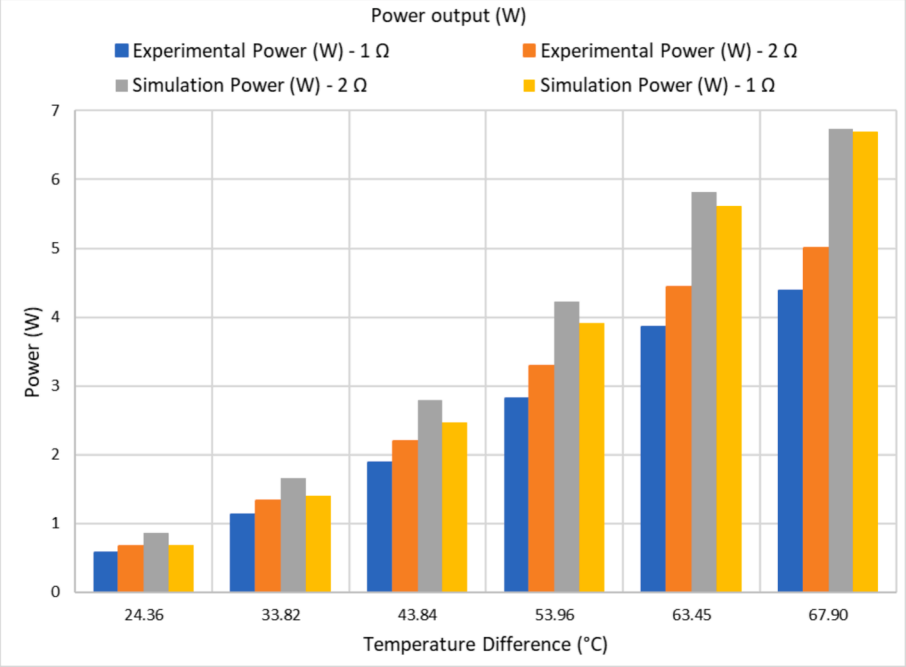

Fig. 16. Power generated from the experimental test rig and the computational simulation.

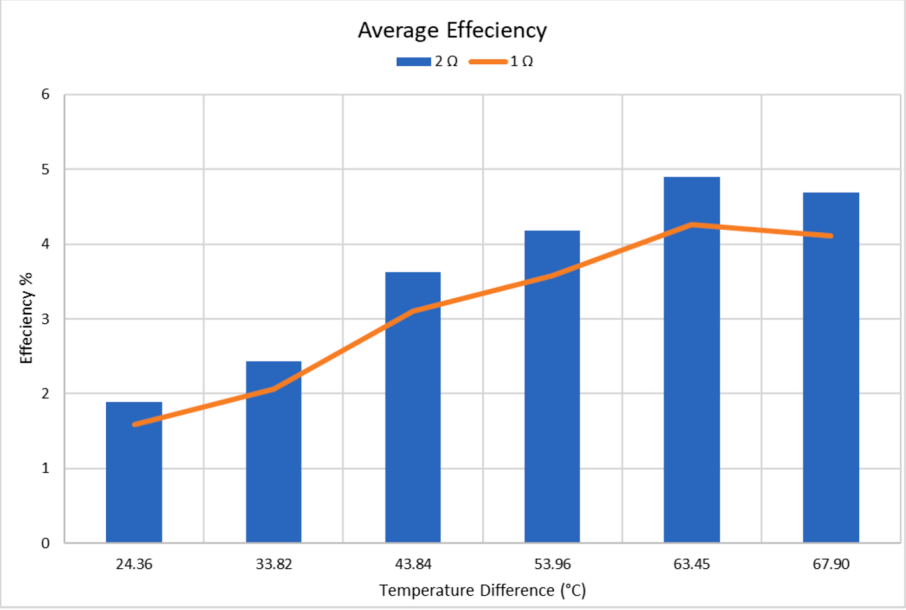

Fig. 17. Average efficiency of test rig for 1 Ω Vs 2 Ω.

generated from the computational model alongside the experimental counterpart in open circuit, while Figs. 13 and 14 depict the scenarios in closed circuit with external loads of 1 Ω and 2 Ω, respectively. These figures offer a comparative insight into the electrical potential variations under different operating conditions.

To validate the computational model, the electrical distribution data obtained from the computational investigation was compared with the data collected from the experimental test rig. Fig. 15 illustrates the relative error associated with the voltage potential between the experimental and computational simulation results. The figure highlights that the open circuit simulation exhibited the least relative error, with an average relative error of 5 %. In contrast, the closed-circuit simulations at 1 Ω and 2 Ω displayed average relative errors of 12.56 % and 12.14 %, respectively.

The low relative errors across these simulations indicate a strong agreement between the results obtained from the computational model and those from the experimental test rig. This robust agreement serves as a validation of the computational model, reinforcing its accuracy and reliability in simulating the electrical distribution in the thermoelectric generator system.

5.3. *Power generation and efficiency*

With external loads of 1 Ω and 2 Ω applied, the power generated by the thermoelectric generator can also be determined.

Fig. 16 illustrates the power generated in the experimental test rig as

well as from the computational simulation. Notably, the figure reveals that the power output at 2 Ω surpasses the power output at 1 Ω. This observation is attributed to the principle that the maximum power output in thermoelectric generators is achieved when the external load matches the internal load at 2 Ω [49]. Moreover, the power output generated from the computational simulation is higher than experimental ones, hence the voltage potential of it was higher than the experimental voltage potential.

In examining the efficiency performance of the thermoelectric generator, a notable distinction is observed when connected to different external loads. Specifically, the system exhibits a higher efficiency when connected to a 2 Ω external load in comparison to a 1 Ω load. This suggests a dependency of efficiency on the external load resistance, a critical factor influencing the overall performance of the system.

As can be seen from Fig. 17, as the temperature difference increases, the system demonstrates a consistent improvement in efficiency. This positive correlation highlights the significance of temperature difference in optimising the thermoelectric generator's efficiency. However, it is noteworthy that around 70 °C, a slight drop in efficiency is observed. This deviation prompts further investigation into potential operational limits in the system's behaviour at higher temperatures.

In summarizing the efficiency data, the average efficiency for the 1 Ω load is calculated at 3.12 %, while the average efficiency for the 2 Ω load increases to 3.62 %.

6. Conclusion

An innovative aspect of this research is the development and validation of a robust computational model, a critical contribution to the field of thermoelectric generators (TEGs). Leveraging COMSOL Multiphysics 6.0, the designed TEG model underwent comprehensive simulations under various conditions. The model's validation against experimental data shows a high level of consistency between simulated and real-world outcomes. The detailed comparison highlights an average relative error of 5 % in open circuit simulations and 12.56 % and 12.14 % in closed-circuit simulations with 1 Ω and 2 Ω external loads, respectively. Notably, the detailed error propagation and uncertainty analysis, standard yet essential components of experimental studies, further reinforce the accuracy of the results. For instance, in determining heat transfer rates, the maximum relative error is quantified at 1.15 % for the hot side and 1.67 % for the cold side.

Power generation analysis reveals that the highest power output occurs when the external load matches the internal load resistance, emphasizing the critical role of load resistance. The computational model validates this observation, aligning closely with experimental findings. Specifically, the average relative error in power output between computational and experimental results is 4.8 %.

The investigation into efficiency underscores a direct correlation with external load resistance. Notably, the average efficiency reaches 3.12 % with a 1 Ω load and rises to 3.62 % with a 2 Ω load. This observation emphasizes the critical significance of aligning external load resistance with internal one for maximizing the performance of thermoelectric generators, confirming that the TEG operates at its peak efficiency when the external resistance matches the internal resistance.

This study shows a validated computational model within the thermoelectric research field but also highlights the necessity of experimental validation for real-world applicability.

Overall, this study has successfully achieved its aim of conducting a comprehensive investigation into the thermoelectric phenomenon using a 3-dimensional computational model of TEGs developed in COMSOL Multiphysics 6.0. The research focused on integrating thermal and electrical models to explore temperature and electrical distribution, power output, and efficiency of the TEG under various temperature gradients. Through systematic simulations and experimental analyses, the study has contributed valuable insights for optimizing TEG performance and advancing understanding of their potential in harnessing low-grade heat for electricity generation. Furthermore, the precision development of the presented computational model and its alignment with experimental results provide a robust framework for future studies in thermoelectric energy conversion.

CRediT authorship contribution statement

Qusay Doraghi: Writing – original draft, Methodology, Formal analysis, Data curation. **Hussam Jouhara:** Writing – review & editing, Resources, Methodology, Investigation, Funding acquisition, Conceptualization.

Declaration of competing interest

The authors declare that they have no known competing financial interests or personal relationships that could have appeared to influence the work reported in this paper.

Data availability

Data will be made available on request.

References

[1] A. Baroutaji, et al., Advancements and prospects of thermal management and waste heat recovery of PEMFC, Int. J. Thermofluids 9 (2021) 100064, https://doi.org/10.1016/j.ijft.2021.100064.
[2] H. Jaber, A. Herez, T. Lemenand, M. Ramadan, M. Khaled, Experimental study on heat recovery from exhaust gas of chimneys using multi-tube tank: effect of changing the head shape, Int. J. Thermofluids 20 (2023) 100518, https://doi.org/10.1016/j.ijft.2023.100518.
[3] D. Brough, H. Jouhara, The aluminium industry: a review on state-of-the-art technologies, environmental impacts and possibilities for waste heat recovery, Int. J. Thermofluids 1–2 (2020) 100007, https://doi.org/10.1016/j.ijft.2019.100007.
[4] International Energy Agency, International Energy Agency (IEA) World Energy Outlook 2022, Int. Energy Agency, p. 524, 2022, [Online]. Available: https://www.iea.org/reports/world-energy-outlook-2022.
[5] I. Energy Agency, Net Zero by 2050 – A Roadmap for the Global Energy Sector," 2050, Accessed: Sep. 21, 2023. [Online]. Available: www.iea.org/t&c/.
[6] R. Freer, A.V. Powell, Realising the potential of thermoelectric technology: a roadmap, J. Mater. Chem. C 8 (2) (2020) 441–463, https://doi.org/10.1039/C9TC05710B.
[7] Y. Zhang, et al., High-temperature and high-power-density nanostructured thermoelectric generator for automotive waste heat recovery, Energy Convers. Manag. 105 (2015) 946–950, https://doi.org/10.1016/j.enconman.2015.08.051.
[8] R.-C. Talawo, B.E.M. Fotso, M. Fogue, An experimental study of a solar thermoelectric generator with vortex tube for hybrid vehicle, Int. J. Thermofluids 10 (2021) 100079, https://doi.org/10.1016/j.ijft.2021.100079.
[9] K.A. Kuterbekov, A.M. Kabyshev, K.Z. Bekmyrza, M.M. Kubenova, A. Aghajani, Experimental evaluation of combined humidifier-dehumidifier desalination with thermoelectric module for simultaneous use of heating and cooling, Int. J. Thermofluids 21 (2024) 100560. doi: 10.1016/j.ijft.2024.100560.
[10] M. Ge, Y. Zhao, Y. Li, W. He, L. Xie, Y. Zhao, Structural optimization of thermoelectric modules in a concentration photovoltaic–thermoelectric hybrid system, Energy 244 (2022) 123202, https://doi.org/10.1016/J.ENERGY.2022.123202.
[11] D. Luo, Z. Sun, R. Wang, Performance investigation of a thermoelectric generator system applied in automobile exhaust waste heat recovery, Energy 238 (2022) 121816, https://doi.org/10.1016/J.ENERGY.2021.121816.
[12] H. Jouhara, et al., Thermoelectric generator (TEG) technologies and applications, Int. J. Thermofluids 9 (2021) 100063, https://doi.org/10.1016/j.ijft.2021.100063.
[13] Y. Du, et al., Boosting thermoelectric generator (TEG) performance with tandem radiative/evaporative/phase change cooler, Nano Energy 128 (2024) 109909, https://doi.org/10.1016/j.nanoen.2024.109909.
[14] M.A. Abdelkareem, et al., Prospects of thermoelectric generators with nanofluid, Therm. Sci. Eng. Prog. 29 (2022) 101207, https://doi.org/10.1016/J.TSEP.2022.101207.
[15] Y. Zhao, Y. Fan, W. Li, Y. Li, M. Ge, L. Xie, Experimental investigation of heat pipe thermoelectric generator, Energy Convers. Manag. 252 (2022) 115123, https://doi.org/10.1016/J.ENCONMAN.2021.115123.
[16] H. Hazama, Y. Masuoka, A. Suzumura, M. Matsubara, S. Tajima, R. Asahi, Cylindrical thermoelectric generator with water heating system for high solar energy conversion efficiency, Appl. Energy 226 (2018) 381–388, https://doi.org/10.1016/J.APENERGY.2018.06.015.
[17] F. Suarez, A. Nozariasbmarz, D. Vashaee, M.C. Öztürk, Designing thermoelectric generators for self-powered wearable electronics, Energy Environ. Sci. 9 (6) (2016) 2099–2113, https://doi.org/10.1039/C6EE00456C.

[18] A. Nozariasbmarz, et al., Review of wearable thermoelectric energy harvesting: from body temperature to electronic systems, Appl. Energy 258 (2020) 114069, https://doi.org/10.1016/J.APENERGY.2019.114069.
[19] M. Ge, et al., Experimental study on thermoelectric power generation based on cryogenic liquid cold energy, Energy 220 (2021) 119746, https://doi.org/10.1016/J.ENERGY.2020.119746.
[20] M. He, E. Wang, Y. Zhang, W. Zhang, F. Zhang, C. Zhao, Performance analysis of a multilayer thermoelectric generator for exhaust heat recovery of a heavy-duty diesel engine, Appl. Energy 274 (2020) 115298, https://doi.org/10.1016/J.APENERGY.2020.115298.
[21] A.G. Olabi, et al., Potential applications of thermoelectric generators (TEGs) in various waste heat recovery systems, Int. J. Thermofluids 16 (2022) 100249, https://doi.org/10.1016/j.ijft.2022.100249.
[22] A. Anderson, B. Rezaie, Geothermal technology: trends and potential role in a sustainable future, Appl. Energy 248 (2019) 18–34, https://doi.org/10.1016/J.APENERGY.2019.04.102.
[23] M. Bozorgi, P. Roy, A.R.M. Siddique, K. Venkateshwar, S. Tasnim, S. Mahmud, Experimental investigation and life cycle assessment of a phase change material (PCM) based thermoelectric (TE) refrigerator, Int. J. Thermofluids 19 (2023) 100394, https://doi.org/10.1016/j.ijft.2023.100394.
[24] Y. Zhao, X. Yan, Y. Fan, M. Ge, L. Yue, S. Wang, Analysis of optimal humidification temperature for a flue gas thermoelectric generation system with gas humidification, J. Clean. Prod. 285 (2021) 125467, https://doi.org/10.1016/J.JCLEPRO.2020.125467.
[25] M.A. Mansour, et al., Effect of liquid saturated porous medium on heat transfer from thermoelectric generator, Int. J. Thermofluids 17 (2023) 100264, https://doi.org/10.1016/j.ijft.2022.100264.
[26] H. Jouhara, N. Khordehgah, S. Almahmoud, B. Delpech, A. Chauhan, S.A. Tassou, Waste heat recovery technologies and applications, Therm. Sci. Eng. Prog. 6 (2018) 268–289, https://doi.org/10.1016/J.TSEP.2018.04.017.
[27] S. Vostrikov, A. Somov, P. Gotovtsev, M. Magno, Comprehensive modelling framework for a low temperature gradient thermoelectric generator, Energy Convers. Manag. 247 (2021) 114721, https://doi.org/10.1016/J.ENCONMAN.2021.114721.
[28] S. Vostrikov, A. Somov, P. Gotovtsev, Low temperature gradient thermoelectric generator: modelling and experimental verification, Appl. Energy 255 (2019) 113786.
[29] Q. Doraghi, et al., Investigation and computational modelling of variable TEG leg geometries, ChemEngineering 5(3) (2021). doi: 10.3390/chemengineering5030045.
[30] A. Eldesoukey, H. Hassan, 3D model of thermoelectric generator (TEG) case study: effect of flow regime on the TEG performance, Energy Convers. Manag. 180 (2019) 231–239, https://doi.org/10.1016/J.ENCONMAN.2018.10.104.
[31] Q. Doraghi, A. Żabnieńska-Góra, L. Norman, B. Krause, P. Pötschke, H. Jouhara, Experimental and computational analysis of thermoelectric modules based on melt-mixed polypropylene composites, Therm. Sci. Eng. Prog. 39 (2023) 101693, https://doi.org/10.1016/J.TSEP.2023.101693.
[32] Q. Doraghi, et al., Experimental and computational thermoelectric generator for waste heat recovery for aeronautic application, Energy 297 (2024) 131286, https://doi.org/10.1016/j.energy.2024.131286.
[33] D. Luo, R. Wang, Y. Yan, Z. Sun, W. Zhou, R. Ding, Comparison of different fluid-thermal-electric multiphysics modeling approaches for thermoelectric generator systems, Renew. Energy 180 (2021) 1266–1277, https://doi.org/10.1016/J.RENENE.2021.09.033.
[34] L. Ga, S. Huang, Y. Zhang, D. Xu, W. Li, Thermal resistances model for a soil-to-air thermoelectric generator device, Case Stud. Therm. Eng. 39 (2022) 102475, https://doi.org/10.1016/J.CSITE.2022.102475.
[35] A.K. Menon, S.K. Yee, Design of a polymer thermoelectric generator using radial architecture, J. Appl. Phys. 119 (5) (2016) 055501, https://doi.org/10.1063/1.4941101.
[36] M. Ge, Z. Li, Y. Zhao, Z. Xuan, Y. Li, Y. Zhao, Experimental study of thermoelectric generator with different numbers of modules for waste heat recovery, Appl. Energy 322 (2022) 119523, https://doi.org/10.1016/J.APENERGY.2022.119523.
[37] L.S. Hewawasam, A.S. Jayasena, M.M.M. Afnan, R.A.C.P. Ranasinghe, M. A. Wijewardane, Waste heat recovery from thermo-electric generators (TEGs), Energy Rep. 6 (2020) 474–479, https://doi.org/10.1016/j.egyr.2019.11.105.
[38] X. Wang, et al., An optimized design approach concerning thermoelectric generators with frustum-shaped legs based on three-dimensional multiphysics model, Energy 233 (2021) 120810, https://doi.org/10.1016/J.ENERGY.2021.120810.
[39] Thermoelectric Power Generator (TEG) Module 62 x 62mm 15.6W. https://www.europeanthermodynamics.com/products/thermoelectric-modules/seebeck-generator/power-generation-module-62-x-62mm-15-6w-gm200-127-28-12 (accessed Jan. 16, 2024).
[40] F. Products, R. Articles, How to fit a thermoelectric module introduction, no. 2, 2019, pp. 1–6.
[41] T.I. Sheets, RS PRO Thermal Insulation, pp. 1–3.
[42] Q. Zhao, J. Li, H. Zhang, Synergizing perovskite solar cell and thermoelectric generator for broad-spectrum utilization: model updating, performance assessment and optimization, Energy 289 (2024) 130008, https://doi.org/10.1016/J.ENERGY.2023.130008.
[43] A. Jafari, M. Vahab, P. Broumand, N. Khalili, An eXtended finite element method implementation in COMSOL multiphysics: thermo-hydro-mechanical modeling of fluid flow in discontinuous porous media, Comput. Geotech. 159 (2023) 105458, https://doi.org/10.1016/j.compgeo.2023.105458.
[44] A.B. Comsol, Introduction to COMSOL multiphysics, Version 4 (2018) 1998–2010.
[45] A. Draper, N. McKibben, D. Estrada, Z. Deng, Multiphysics modeling of printed surface acoustic wave thermometers, Sens. Actuators A Phys. 359 (2023) 114491, https://doi.org/10.1016/j.sna.2023.114491.
[46] V. Gerlich, K. Sulovská, M. Zálešák, COMSOL Multiphysics validation as simulation software for heat transfer calculation in buildings: building simulation software validation, Measurement 46 (6) (2013) 2003–2012, https://doi.org/10.1016/j.measurement.2013.02.020.
[47] J.H. Meng, X.X. Zhang, X.D. Wang, Characteristics analysis and parametric study of a thermoelectric generator by considering variable material properties and heat losses, Int. J. Heat Mass Transf. 80 (Jan. 2015) 227–235, https://doi.org/10.1016/J.IJHEATMASSTRANSFER.2014.09.023.
[48] Comsol, COMSOL Multiphysics Application Library, Accessed: Aug. 18, 2022. [Online]. Available: www.comsol.com/trademarks.
[49] O.I. Ibeagwu, Modelling and comprehensive analysis of TEGs with diverse variable leg geometry, Energy 180 (2019) 90–106, https://doi.org/10.1016/j.energy.2019.05.088.